An antiangiogenic isoform of VEGF-A contributes to impaired vascularization in peripheral artery disease

Ryosuke Kikuchi[1,2], Kazuto Nakamura[1], Susan MacLauchlan[1], Doan Thi-Minh Ngo[3], Ippei Shimizu[1], Jose Javier Fuster[1], Yasufumi Katanasaka[1], Sumiko Yoshida[1], Yan Qiu[4], Terry P Yamaguchi[5], Tadashi Matsushita[6], Toyoaki Murohara[7], Noyan Gokce[3], David O Bates[4,8], Naomi M Hamburg[1,9] & Kenneth Walsh[1]

Peripheral artery disease (PAD) generates tissue ischemia through arterial occlusions and insufficient collateral vessel formation. Vascular insufficiency in PAD occurs despite higher circulating levels of vascular endothelial growth factor A (VEGF-A)[1,2], a key regulator of angiogenesis. Here we show that clinical PAD is associated with elevated levels of an antiangiogenic VEGF-A splice isoform (VEGF-A$_{165}$b) and a corresponding reduction in levels of the proangiogenic VEGF-A$_{165}$a splice isoform. In mice, VEGF-A$_{165}$b expression was upregulated by conditions associated with impaired limb revascularization, including leptin deficiency, diet-induced obesity, genetic ablation of the secreted frizzled-related protein 5 (Sfrp5) adipokine and transgenic overexpression of Wnt5a in myeloid cells. In a mouse model of PAD, delivery of VEGF-A$_{165}$b inhibited revascularization of ischemic hind limbs, whereas treatment with an isoform-specific neutralizing antibody reversed impaired revascularization caused by metabolic dysfunction or perturbations in the Wnt5a-Sfrp5 regulatory system. These results indicate that inflammation-driven expression of the antiangiogenic VEGF-A isoform can contribute to impaired collateralization in ischemic cardiovascular disease.

Disability attributable to PAD is rising because of an aging population and an increase in the prevalence of metabolic diseases[3]. Lower-extremity ischemia in PAD is painful, disabling, causes nonhealing ulcers and results in 200,000 amputations per year in the United States alone[4,5]. PAD is thus a major unmet clinical need afflicting approximately 10 million people in the United States[6]. Limb ischemia induced by arterial obstructive lesions is exacerbated by insufficient angiogenesis and collateral vessel formation[7], processes that are regulated by VEGF-A[8]. Paradoxically, VEGF-A levels are reported to be elevated in patients with advanced PAD[2,9]. Furthermore, clinical interventions to promote therapeutic angiogenesis by VEGF-A delivery have had

limited efficacy in PAD[10,11]. It is therefore not clear why collateralization and angiogenesis are insufficient in patients with PAD despite raised VEGF-A levels.

Recent work in cancer biology has identified splice variants of human VEGF-A that inhibit angiogenesis[12–15]. These isoforms arise from differential splicing of exon 8: proximal splice site usage results in an mRNA containing the initial 19 nucleotides of exon 8a, coding for the proangiogenic VEGF-A$_{165}$a protein in humans, whereas distal splice site usage results in expression of exon 8b and the antiangiogenic family of isoforms typified by VEGF-A$_{165}$b (**Fig. 1b**). VEGF-A$_{165}$b inhibits canonical VEGF-A signaling by competitive interference with the interaction of proangiogenic isoforms with the VEGF receptor 2 (VEGFR2)–neuropilin 1 (NRP1) receptor complex, thereby preventing full downstream signaling of VEGFR2 (refs. 13,16). However, the relevance of inhibitory VEGF-A variants to clinical ischemic syndromes, including PAD, remains incompletely defined[17], and the existence of mouse VEGF-A$_{165}$b has been questioned[18]. More recently, it has been reported that *VEGFA* mRNA undergoes a translational readthrough event, generating an isoform referred to as VEGF-Ax that contains a 22-amino-acid extension that encompasses exons 8a and 8b and utilizes the exon 8b stop codon[19]. Thus, there is increasing evidence to suggest that regulatory events at the 3′ end of the *VEGFA* gene are required for precise physiological control of VEGF-A expression.

Consistent with previous reports[2,9], we observed higher levels of circulating VEGF-A in patients with PAD compared to controls using an ELISA that does not discriminate between the VEGF-A isoforms (**Fig. 1a** and **Supplementary Table 1**). To examine the relative presence of the VEGF-A isoform families in patients with PAD, we measured serum levels by immunoblots using antibodies designed to recognize specific epitopes encoded by exons 8a and 8b (**Fig. 1b**). We also determined total VEGF-A levels with a pan–VEGF-A antibody, that does not discriminate between isoforms, directed against the N-terminal portion of the molecule. Consistent with

[1]Molecular Cardiology and Whitaker Cardiovascular Institute, Boston University School of Medicine, Boston, Massachusetts, USA. [2]Department of Medical Technique, Nagoya University Hospital, Nagoya, Aichi, Japan. [3]Clinical Cardiology, Department of Medicine and Whitaker Cardiovascular Institute, Boston University School of Medicine, Boston, Massachusetts, USA. [4]Microvascular Research Laboratories, School of Physiology and Pharmacology, University of Bristol, Bristol, UK. [5]Cancer and Developmental Biology Laboratory, National Cancer Institute, National Institutes of Health, Frederick, Maryland, USA. [6]Department of Clinical Laboratory, Nagoya University Hospital, Nagoya, Aichi, Japan. [7]Department of Cardiology, Nagoya University Graduate School of Medicine, Nagoya, Aichi, Japan. [8]Cancer Biology, Division of Cancer and Stem Cells, School of Medicine, University of Nottingham, Queen's Medical Centre, Nottingham, UK. [9]Evans Department of Medicine and the Whitaker Cardiovascular Institute, Boston University School of Medicine, Boston, Massachusetts, USA. Correspondence should be addressed to K.W. (kxwalsh@bu.edu).
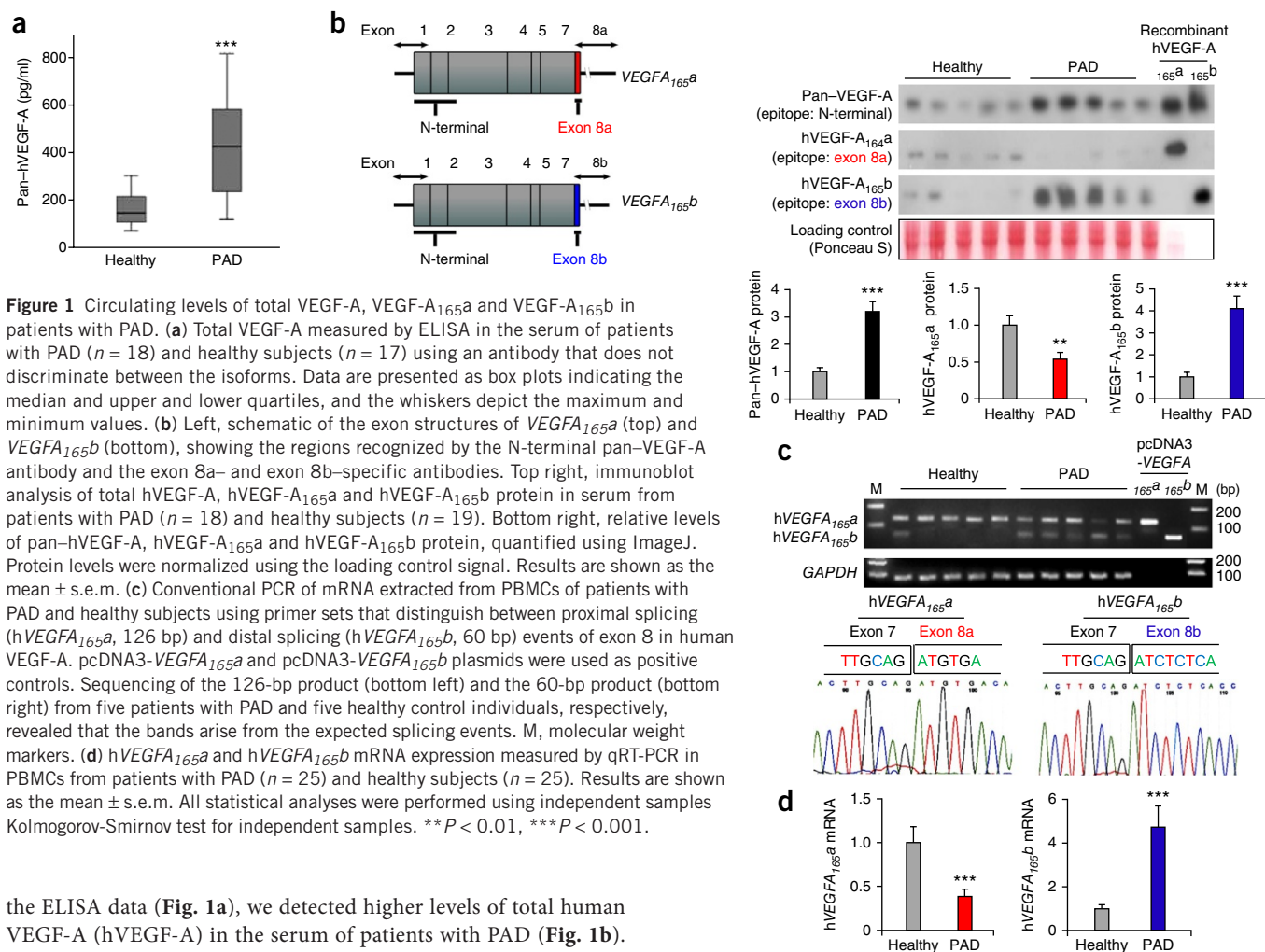
Figure 1 Circulating levels of total VEGF-A, VEGF-A$_{165}$a and VEGF-A$_{165}$b in patients with PAD. (**a**) Total VEGF-A measured by ELISA in the serum of patients with PAD ($n = 18$) and healthy subjects ($n = 17$) using an antibody that does not discriminate between the isoforms. Data are presented as box plots indicating the median and upper and lower quartiles, and the whiskers depict the maximum and minimum values. (**b**) Left, schematic of the exon structures of $VEGFA_{165}a$ (top) and $VEGFA_{165}b$ (bottom), showing the regions recognized by the N-terminal pan–VEGF-A antibody and the exon 8a– and exon 8b–specific antibodies. Top right, immunoblot analysis of total hVEGF-A, hVEGF-A$_{165}$a and hVEGF-A$_{165}$b protein in serum from patients with PAD ($n = 18$) and healthy subjects ($n = 19$). Bottom right, relative levels of pan–hVEGF-A, hVEGF-A$_{165}$a and hVEGF-A$_{165}$b protein, quantified using ImageJ. Protein levels were normalized using the loading control signal. Results are shown as the mean ± s.e.m. (**c**) Conventional PCR of mRNA extracted from PBMCs of patients with PAD and healthy subjects using primer sets that distinguish between proximal splicing (h$VEGFA_{165}a$, 126 bp) and distal splicing (h$VEGFA_{165}b$, 60 bp) events of exon 8 in human VEGF-A. pcDNA3-$VEGFA_{165}a$ and pcDNA3-$VEGFA_{165}b$ plasmids were used as positive controls. Sequencing of the 126-bp product (bottom left) and the 60-bp product (bottom right) from five patients with PAD and five healthy control individuals, respectively, revealed that the bands arise from the expected splicing events. M, molecular weight markers. (**d**) h$VEGFA_{165}a$ and h$VEGFA_{165}b$ mRNA expression measured by qRT-PCR in PBMCs from patients with PAD ($n = 25$) and healthy subjects ($n = 25$). Results are shown as the mean ± s.e.m. All statistical analyses were performed using independent samples Kolmogorov-Smirnov test for independent samples. **$P < 0.01$, ***$P < 0.001$.

the ELISA data (**Fig. 1a**), we detected higher levels of total human VEGF-A (hVEGF-A) in the serum of patients with PAD (**Fig. 1b**). Levels of the proangiogenic hVEGF-A$_{165}$a isoform were reduced in patients with PAD relative to healthy control subjects, whereas levels of the hVEGF-A$_{165}$b isoform were higher in the PAD cohort (**Fig. 1b**). Higher expression of the inhibitory VEGF-A$_{165}$b isoform was associated with lower ankle-brachial index, which is used to assess the severity of PAD (**Supplementary Fig. 1**).

Multiple lines of evidence suggest that inflammatory cell activation contributes to the development and clinical expression of PAD[20,21]. Thus, we determined the transcript levels of h$VEGFA_{165}a$ isoforms in peripheral blood mononuclear cells (PBMCs) isolated from either patients with PAD or healthy control individuals. This analysis employed conventional RT-PCR and a primer set that amplifies a region of the common $VEGFA$ 3′ untranslated region (UTR). We were able to identify the two VEGF-A mRNA isoforms using the predicted differences in the lengths of the PCR products corresponding to $VEGFA_{165}a$ and $VEGFA_{165}b$ stemming from use of the proximal or distal splice sites. The shorter 60-bp fragment, predicted to generate the exon 8b–containing isoform, was preferentially represented in the PBMCs of patients with PAD (**Fig. 1c**). In contrast, PBMCs from healthy control patients predominantly produced a 126-bp PCR fragment, consistent with use of the proximal splice site that incorporates the 8a exon. Sequence analysis of the 126-bp and 60-bp PCR products confirmed the predicted exon 7/8a and 7/8b junctions, respectively (**Fig. 1c**). We then performed quantitative RT-PCR (qRT-PCR) using different primer sets that specifically amplify either exon 8a– or exon 8b–containing transcripts (**Fig. 1d**). This analysis revealed a 61% decrease

in levels of the h$VEGFA_{165}a$ transcript and a 4.6-fold increase in levels of the h$VEGFA_{165}b$ transcript in the PBMCs of patients with PAD relative to healthy control individuals. Higher PBMC expression of the $VEGFA_{165}b$ transcript was strongly associated with higher serum levels of VEGF-A$_{165}$b ($r = 0.65$, $P < 0.0001$; data not shown).

Emerging evidence links noncanonical Wnt5a signaling to the control of vascularization in mouse retinas through changes in the splice pattern of $VEGFR1$, giving rise to soluble fms-like tyrosine kinase-1 (sFlt-1) that functions as a negative regulator of angiogenesis[22,23]. To evaluate the potential involvement of noncanonical WNT signaling in VEGF-A splicing, we assessed $WNT5A$ levels in PBMCs from healthy controls and patients with PAD. We detected higher levels of $WNT5A$ gene expression in PBMCs from patients with PAD compared to those from controls (**Supplementary Fig. 2a**) but similar levels of $sFLT1$ (**Supplementary Fig. 2b**). To identify the cell population accountable for the increased $WNT5A$ gene expression in PBMCs of patients with PAD, we separated two major cellular fractions, monocytes and non-monocytes, from the PBMC samples for a subset of patients and healthy controls. In both subject groups, $WNT5A$ gene expression was higher in the monocyte compared to the non-monocyte fraction, suggesting that $WNT5A$ is more highly expressed in cells of the monocyte and macrophage lineage (**Supplementary Fig. 2c**). In addition, $WNT5A$ transcript levels in circulating monocytes were upregulated in patients with PAD compared with healthy controls,

similar to observations in whole PBMCs samples. Consistent with the concept that *WNT5A* signaling regulates VEGF-A isoform levels, *WNT5A* expression in PBMCs was positively associated with serum levels of VEGF-A$_{165}$b (**Supplementary Fig. 3a**) and was negatively associated with ankle-brachial index (**Supplementary Fig. 3b**).

To investigate whether Wnt5a is functionally relevant to the control of alternative splicing of *Vegfa* in ischemia-induced regenerative angiogenesis, we employed a mouse model of PAD. In this model, PAD is simulated by unilateral resection of the femoral artery, which leads to a hemodynamic deficit that can be monitored noninvasively by laser Doppler blood flow (LDBF) imaging and anatomically by measuring capillary density. We observed a relatively modest upregulation of Wnt5a in the ischemic limbs of wild-type (WT) C57BL/6J mice at both the protein and mRNA levels (**Supplementary Fig. 4a,b**). Immunohistochemical analyses of the ischemic limbs revealed Wnt5a colocalization with cells positive for the macrophage marker protein Mac2 (also called galectin-3 or Lgals3), indicating that macrophages are a source of Wnt5a in this model (**Supplementary Fig. 4c**).

To examine the involvement of Wnt5a in the regulation of *Vegfa* splicing, we constructed mice overexpressing Wnt5a in myeloid cells by crossing lysozyme M–Cre (LysM-Cre) mice with knock-in mice carrying a Cre-inducible Wnt5a transgene, resulting in LysM-Wnt5a^{GOF} mice (GOF, gain of function) (**Supplementary Fig. 5a**). Compared with WT mice, LysM-Wnt5a^{GOF} mice expressed higher levels of Wnt5a protein and mRNA in hind limbs after ischemic surgery (**Supplementary Fig. 5b,c**), which was associated with increased expression of Mac2 (**Supplementary Fig. 5d**), implying an increase in the number of macrophages. Although LysM-Wnt5a^{GOF} mice displayed no detectable baseline phenotype, they had impaired revascularization as determined by LDBF imaging in response to surgical ischemia (**Fig. 2a**). Correspondingly, the gastrocnemius muscle of Wnt5a transgenic mice displayed an inability to increase capillary density in response to ischemia, as assessed in histological sections stained with antibody to CD31 (platelet/endothelial cell adhesion molecule 1, also called PECAM1; **Fig. 2b**) or isolectin IB4 (data not shown). Consistent with the findings in human PAD, serum levels of total VEGF-A were elevated in LysM-Wnt5a^{GOF} mice at 7 days after surgery, as determined by an ELISA that does not discriminate between isoforms (**Fig. 2c**). Using a pan–VEGF-A antibody, western blot analysis of gastrocnemius muscle also revealed an increase in tissue levels of total VEGF-A in response to ischemia, which was further amplified in Wnt5a transgenic mice (**Fig. 2d**). Employing an antibody that specifically recognizes the previously reported amino acid sequence encoded by the C-terminal exon, hereafter referred to as mouse exon 8a, we detected an upregulation of VEGF-A$_{164}$a in the ischemic limbs of WT but not LysM-Wnt5a^{GOF} mice. These assays reveal a striking discrepancy between the levels of total VEGF-A and the exon 8a–containing isoform in the ischemic limbs of the transgenic mice. Moreover, despite an increase in total VEGF-A expression in the ischemic limbs of LysM-Wnt5a^{GOF} mice, tyrosine phosphorylation of VEGFR2 was not activated, indicative of impaired VEGF-A signaling under these conditions (**Supplementary Fig. 6**).

Because the structure of the putative mouse VEGF-A$_{165}$b isoform has not been previously described, we constructed PCR primers that span the C-terminal exons and the 3′ UTR region of the *Vegfa* transcript (**Supplementary Fig. 7**). Conventional PCR analysis of mRNA isolated from the ischemic gastrocnemius muscle of WT mice revealed a PCR product fragment of 281 bp, the size expected to be generated from the proangiogenic *Vegfa$_{164}$a* transcript (**Fig. 2e**). Sequence analysis of this fragment confirmed the exon 7/8a splice event that is predicted to encode the previously reported six-amino-acid terminal portion of mouse VEGF-A$_{164}$a (**Fig. 2f**)[24]. In contrast, RT-PCR analysis of limbs from LysM-Wnt5a^{GOF} mice detected a reduction in the levels of the 281-bp fragment and the appearance of a new band at 215 bp (**Fig. 2e**). Sequence analysis of this product revealed that this transcript is derived from use of a distal splice junction, whereby exon 7 is joined to a new exon, hereafter referred to as mouse exon 8b (**Fig. 2f**). Mouse exon 8b contains a seven-amino-acid open reading frame followed by a stop codon, such that this open reading frame is predicted to contribute to translation of a full-length, mature protein that is 165 amino acids in length and is homologous to human VEGF-A$_{165}$b (**Supplementary Fig. 8**), and is hereafter referred to as mVEGF-A$_{165}$b.

Because mouse VEGF-A$_{165}$b has not been previously characterized, we designed and validated qPCR primers specific for the exon junction 7/8a (m*Vegfa$_{164}$a* primers) or 7/8b (m*Vegfa$_{165}$b* primers) (**Supplementary Fig. 9**). As assessed by qRT-PCR analysis, ischemic surgery led to a 70% increase in levels of the *Vegfa$_{164}$a* isoform in the hind limbs of WT mice, but levels of this transcript declined by a factor of three in the transgenic mice overexpressing Wnt5a in myeloid cells (**Supplementary Fig. 10**). In contrast, there was a marked elevation in the expression of the *Vegfa$_{165}$b* isoform in ischemic hind limbs of the transgenic strain. For detection of the protein encoded by the mouse *Vegfa$_{165}$b* transcript, we produced an antibody to the predicted exon 8b hexapeptide. This antibody did not crossreact with the VEGF-A$_{164}$a protein in immunoblot analyses, and detected the exon 8b–encoded epitope in total VEGF-A immunoprecipitated from ischemic hind limbs of the transgenic mice (**Supplementary Fig. 11**). Using this antibody, we found that levels of the exon 8b–containing isoform, i.e., VEGF-A$_{165}$b, were upregulated in the ischemic hind limbs of the transgenic mice (**Fig. 2g**).

We next performed immunoblot analysis using an antibody that recognizes the *VEGFA* translational readthrough product that is referred to as VEGF-Ax (**Supplementary Fig. 12a**). In contrast to our findings with the antibody that recognizes the exon 8b hexapeptide, which is predicted to be present in both the VEGF-A$_{165}$b and VEGF-Ax isoforms, we detected no immunoreactive material in the ischemic limbs of WT or transgenic mice using the antibody that recognizes the highly conserved Ax readthrough peptide that is uniquely present in VEGF-Ax (**Supplementary Fig. 12b**). Because VEGF-Ax is reported to be widely expressed in human tissues[19], we reanalyzed a subset of serum samples from patients with PAD or healthy control subjects using antibodies that specifically recognize the unique readthrough portion of VEGF-Ax or the terminal hexapeptide encoded by exon 8b. This analysis detected Ax peptide–immunoreactive material in the sera of both healthy controls and patients with PAD; however, unlike the exon 8b–specific epitope, there was no difference in the levels of the Ax epitope between the two groups (**Supplementary Fig. 12c**).

To explore the functional importance of mVEGF-A$_{165}$b, we constructed an adenoviral vector expressing this isoform (Ad-m*Vegfa$_{165}$b*) and administered it intravenously to WT mice before hind limb ischemic surgery. Flow recovery in Ad-m*Vegfa$_{165}$b*–treated mice was significantly less than that in control mice by the third day after surgery, and this difference in recovery persisted throughout the time course of the experiment (**Fig. 2h**). Quantitative analysis of CD31-positive cells in gastrocnemius muscle on day 14 after surgery revealed that the ischemia-induced increase in capillary density present in control mice was abrogated in Ad-m*Vegfa$_{165}$b*–treated mice (**Fig. 2h**), corroborating the LDBF imaging data. To assess the function of endogenous mVEGF-A$_{165}$b, we treated LysM-Wnt5a^{GOF}
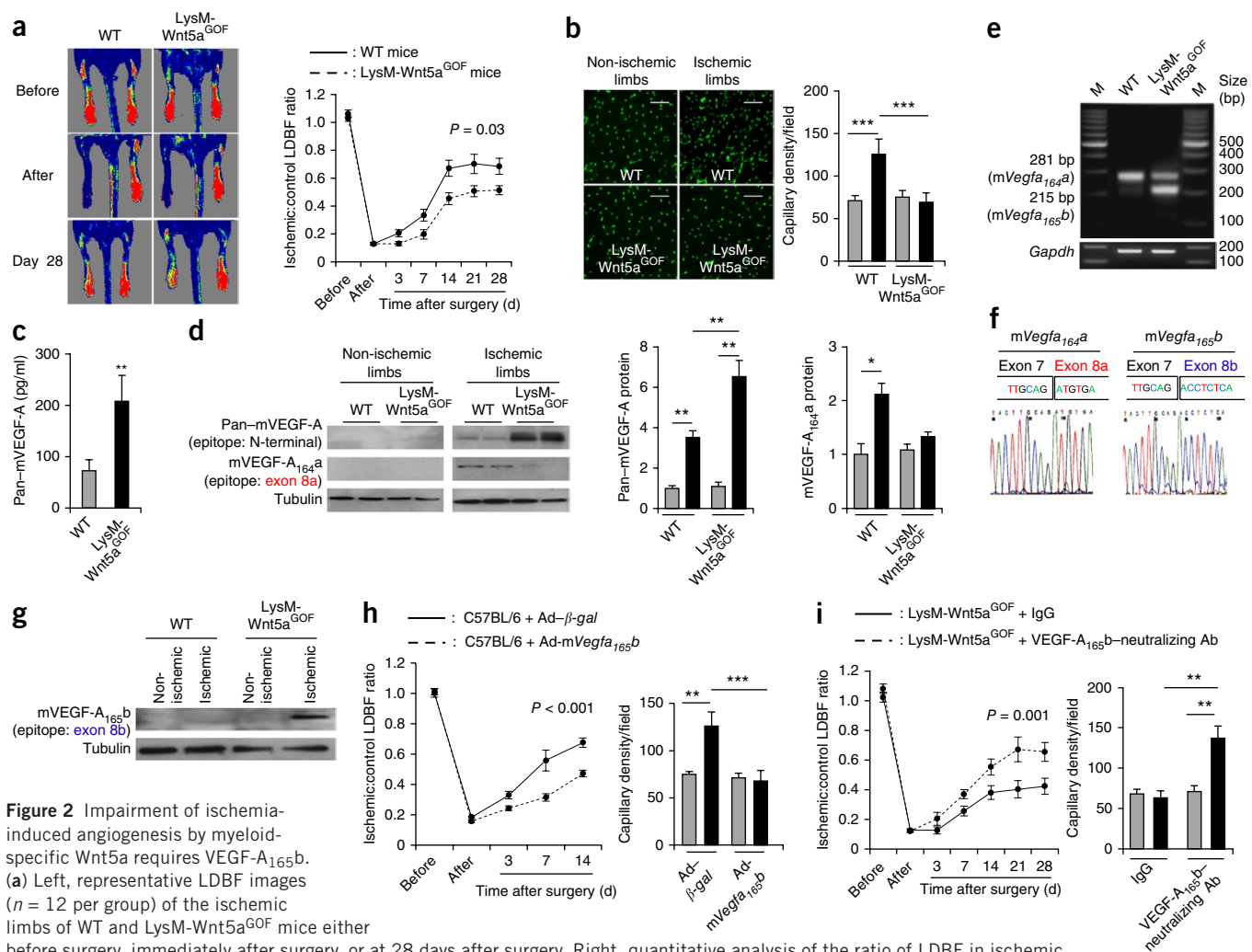
Figure 2 Impairment of ischemia-induced angiogenesis by myeloid-specific Wnt5a requires VEGF-A$_{165}$b. (**a**) Left, representative LDBF images ($n = 12$ per group) of the ischemic limbs of WT and LysM-Wnt5a^{GOF} mice either before surgery, immediately after surgery, or at 28 days after surgery. Right, quantitative analysis of the ratio of LDBF in ischemic limbs compared to non-ischemic limbs (control) in WT and LysM-Wnt5a^{GOF} mice at the indicated time points after surgery. Results are shown as the mean ± s.e.m. ($n = 12$). Statistical significance was calculated by repeated measures analysis of variance (ANOVA). (**b**) Left, immunostaining of the gastrocnemius with monoclonal antibody to CD31 (green in tissue sections) in contralateral non-ischemic (gray bars) and ischemic (black bars) tissue in WT and LysM-Wnt5a^{GOF} mice. Right, quantitative analysis of capillary density at day 28 after surgery. Capillary density is expressed as the number of capillaries per high-power field (×200). Scale bars, 100 μm. Results are shown as the mean ± s.e.m. ($n = 5$ per group). Statistical significance was calculated by ANOVA with *post-hoc* Tukey HSD test. (**c**) Circulating levels of total mVEGF-A in WT and LysM-Wnt5a^{GOF} mice by ELISA employing a pan–mVEGF-A antibody at 7 d after surgery. Results are shown as the mean ± s.e.m. ($n = 8$ per group). Statistical significance was calculated by independent samples *t* test for independent samples. (**d**) Left, total mVEGF-A and mVEGF-A$_{164}$a isoform protein expression determined by immunoblot analysis in contralateral non-ischemic (gray bars) and ischemic (black bars) muscle at 7 d after surgery. A representative blot from three independent experiments is shown. Right, relative levels of total mVEGF-A and mVEGF-A$_{164}$a protein quantified using ImageJ. Protein levels were normalized using tubulin as the loading control. Results are shown as the mean ± s.e.m. ($n = 5$ per group). Statistical significance was calculated by ANOVA with *post-hoc* Tukey HSD test. (**e**) Conventional PCR of mRNA from WT and LysM-Wnt5a^{GOF} gastrocnemius muscle 7 d after hind limb ischemic surgery using primers that span both the proximal and distal splice sites (m*Vegfa$_{164}$a* and m*Vegfa$_{165}$b*, respectively). (**f**) Sequencing traces of the 281-bp (left) and 215-bp (right) PCR products from the agarose gel in **e** in the region of the splice junctions of m*Vegfa$_{164}$a* and m*Vegfa$_{165}$b*. (**g**) mVEGF-A$_{165}$b protein expression determined by immunoblot analysis using an antibody that recognizes the peptide encoded by mouse exon 8b in contralateral non-ischemic (gray bars) and ischemic (black bars) muscle at 7 d after surgery. A representative blot from three independent experiments is shown. (**h**) Left, ischemic to non-ischemic LDBF ratio at the indicated time points after surgery in WT mice injected with Ad-m*Vegfa$_{165}$b* or an adenoviral vector expressing β-galactosidase (Ad–β-*gal*) (control) into the jugular vein (2×10^9 PFU in each group) at 3 d before ischemic hind limb surgery. Results are shown as the mean ± s.e.m. ($n = 10$ per group). Statistical significance was calculated by repeated measures ANOVA. Right, quantitative analysis of capillary density by CD31-specific antibody in Ad-m*Vegfa$_{165}$b*–treated or control mice on day 14 after surgery. Capillary density is expressed as the number of capillaries per high-power field (×200) in the contralateral non-ischemic (gray bars) and ischemic (black bars) limbs. Results are shown as the mean ± s.e.m. ($n = 5$ per group). Statistical significance was calculated by ANOVA with *post-hoc* Tukey HSD test. (**i**) Left, quantitative analysis of the ischemic to non-ischemic LDBF ratio at the indicated time points after surgery in LysM-Wnt5a^{GOF} mice treated intraperitoneally with control IgG or VEGF-A$_{165}$b–neutralizing monoclonal antibody (Ab) (100 μg) on days 0, 3 and 7 after surgery. Results are shown as the mean ± s.e.m. ($n = 10$ per group). Statistical significance was calculated by repeated measures ANOVA. Right, quantitative analysis of capillary density by CD31-specific antibody staining in LysM-Wnt5a^{GOF} mice receiving control IgG or VEGF-A$_{165}$b–neutralizing antibody at day 28 after surgery. Capillary density is expressed as the number of capillaries per high-power field (×200) in the contralateral non-ischemic (gray bars) and ischemic (black bars) limbs. Results are shown as the mean ± s.e.m. ($n = 5$ per group). Statistical significance was calculated by ANOVA with *post-hoc* Tukey HSD test. *$P < 0.05$, **$P < 0.01$, ***$P < 0.001$.

Figure 3 VEGF-A$_{165}$b impairs ischemia-induced angiogenesis in mice with diet-induced obesity. (**a**) Left, Wnt5a protein levels determined by immunoblot analysis in the contralateral non-ischemic (gray bars) and ischemic (black bars) muscle at 3 d after surgery. A representative blot from three independent experiments is shown. Right, relative Wnt5a protein levels quantified using ImageJ. Protein levels were normalized using tubulin as the loading control. Results are shown as the mean ± s.e.m. (*n* = 5 per group). Statistical significance was calculated by ANOVA with *post-hoc* Tukey HSD test. (**b**) *Wnt5a* mRNA expression measured by qRT-PCR in contralateral non-ischemic (gray bars) and ischemic (black bars) muscle at 3 d after surgery. Results are shown as the mean ± s.e.m. (*n* = 5 per group). Statistical significance was calculated by ANOVA with *post-hoc* Tukey HSD test. (**c**) Representative immunostaining for Wnt5a and Mac2 in the ischemic limbs from mice fed standard chow (top) or HF/HS diet (bottom). Scale bars, 100 μm. *n* = 5 per group. (**d**) Left, total mVEGF-A, mVEGF-A$_{164}$a and mVEGF-A$_{165}$b protein levels determined by immunoblot analysis in contralateral non-ischemic (gray bars) and ischemic (black bars) muscle at 7 d after surgery. A representative blot from three independent experiments is shown. Right, relative levels of pan–mVEGF-A, mVEGF-A$_{164}$a and mVEGF-A$_{165}$b protein normalized to the tubulin signal and quantified using ImageJ. Results are shown as the mean ± s.e.m.


(*n* = 5 per group). Statistical significance was calculated by ANOVA with *post-hoc* Tukey HSD test. (**e**) Levels of m*Vegfa$_{164}$a* and m*Vegfa$_{165}$b* mRNA expression measured by qRT-PCR in non-ischemic (gray bars) and ischemic (black bars) muscle at 7 d after surgery. Results are shown as the mean ± s.e.m. (*n* = 5 per group). Statistical significance was calculated by ANOVA with *post-hoc* Tukey HSD test. (**f**) Left, quantitative analysis of the ischemic to non-ischemic LDBF at the indicated time points after surgery in mice with diet-induced obesity treated with control IgG or VEGF-A$_{165}$b–neutralizing antibody (100 μg) on days 0, 3 and 7 after surgery. Results are shown as the mean ± s.e.m. (*n* = 10 per group). Statistical significance was calculated by repeated measures ANOVA with *post-hoc* Tukey HSD test comparing HF/HS + IgG to HF/HS + VEGF-A$_{165}$b–neutralizing antibody (*P* = 0.01) or to standard chow + IgG (*P* < 0.001). Right, quantitative analysis of capillary density in mice with diet-induced obesity treated with control IgG or VEGF-A$_{165}$b–neutralizing antibody at day 28 after surgery. Capillary density is expressed as the number of capillaries per high-power field (×200) in contralateral non-ischemic (gray bars) and ischemic (black bars) muscle. Results are shown as the mean ± s.e.m. (*n* = 5 per group). Statistical significance was calculated by ANOVA with *post-hoc* Tukey HSD test. *P < 0.05, **P < 0.01, ***P < 0.001.

mice, in which the levels of mVEGF-A$_{165}$b are upregulated, with an exon 8b–specific neutralizing antibody delivered intraperitoneally (**Supplementary Fig. 13**), and then subjected the mice to hind limb ischemic surgery. Mice receiving VEGF-A$_{165}$b–neutralizing antibody displayed improved blood flow reperfusion and increased capillary density in the affected limb compared with LysM-Wnt5a^{GOF} mice receiving an equivalent dose of IgG control antibody (**Fig. 2i**). In contrast, WT mice, in which mVEGF-A$_{165}$b expression is not appreciably increased after ischemic surgery, were refractory to treatment with the neutralizing antibody. Collectively, these results show that macrophage expression of Wnt5a inhibits regenerative angiogenesis, at least in part, through upregulation of mVEGF-A$_{165}$b.

The secreted protein Sfrp5 is expressed predominantly by adipose tissue, where it inhibits inflammation by suppressing noncanonical Wnt5a signaling in macrophages[25]. We therefore evaluated the effect of Sfrp5 deficiency on ischemia-induced angiogenesis and VEGF-A$_{165}$b expression. As was observed in LysM-Wnt5a^{GOF} mice, Sfrp5 deficiency led to impaired reperfusion and capillary density of ischemic limbs in the PAD model (**Supplementary Fig. 14a,b**). To assess the molecular basis for the angiogenic deficiency of the Sfrp5 knockout (KO) mice, we used qRT-PCR to analyze the expression

patterns of *Wnt* family members in the ischemic and non-ischemic gastrocnemius muscle of Sfrp5 KO compared to WT mice. Of the 19 *Wnt* family members, only the *Wnt5a* transcript was expressed at a higher level in the ischemic limbs of Sfrp5 KO mice as compared to WT mice (**Supplementary Fig. 14c**). Wnt5a protein expression, as assessed by immunoblot analysis, was also markedly upregulated in the ischemic limb muscle of Sfrp5 KO mice (**Supplementary Fig. 14d**), a result that is attributable to a greater influx of Mac2 and Wnt5a double-positive macrophages (**Supplementary Fig. 14e**). Consistent with these findings, immunoblot analysis revealed that Sfrp5 deficiency led to a marked increase in Mac2 expression in the ischemic limb but had no effect on Mac2 expression in the uninjured contralateral limb (**Supplementary Fig. 14f**). Thus, Sfrp5 deficiency phenocopies myeloid-specific Wnt5a overexpression in its impairment of regenerative angiogenesis and enhancement of macrophage infiltration in ischemic limbs, and Sfrp5 deficiency can be used as another approach to study the role of the mVEGF-A$_{165}$b isoform.

We next used immunoblot analysis to assess total mouse VEGF-A, VEGF-A$_{164}$a and VEGF-A$_{165}$b expression in hind limb muscle from Sfrp5 KO and WT mice. As was observed in LysM-Wnt5a^{GOF} mice, Sfrp5 KO mice showed an increase in total VEGF-A protein
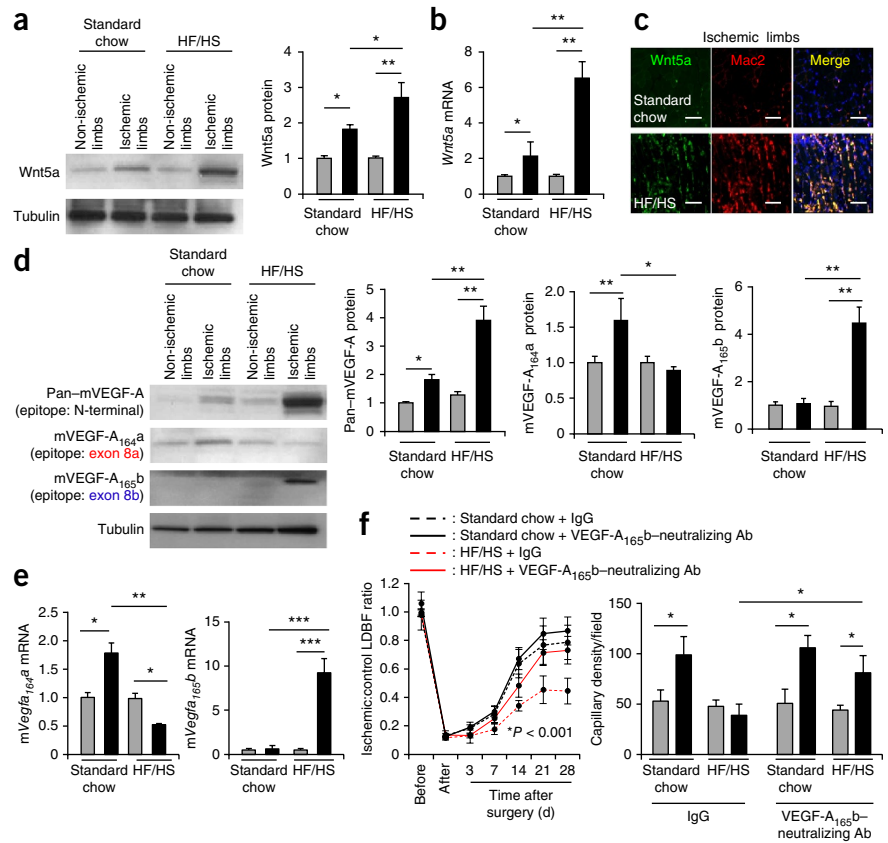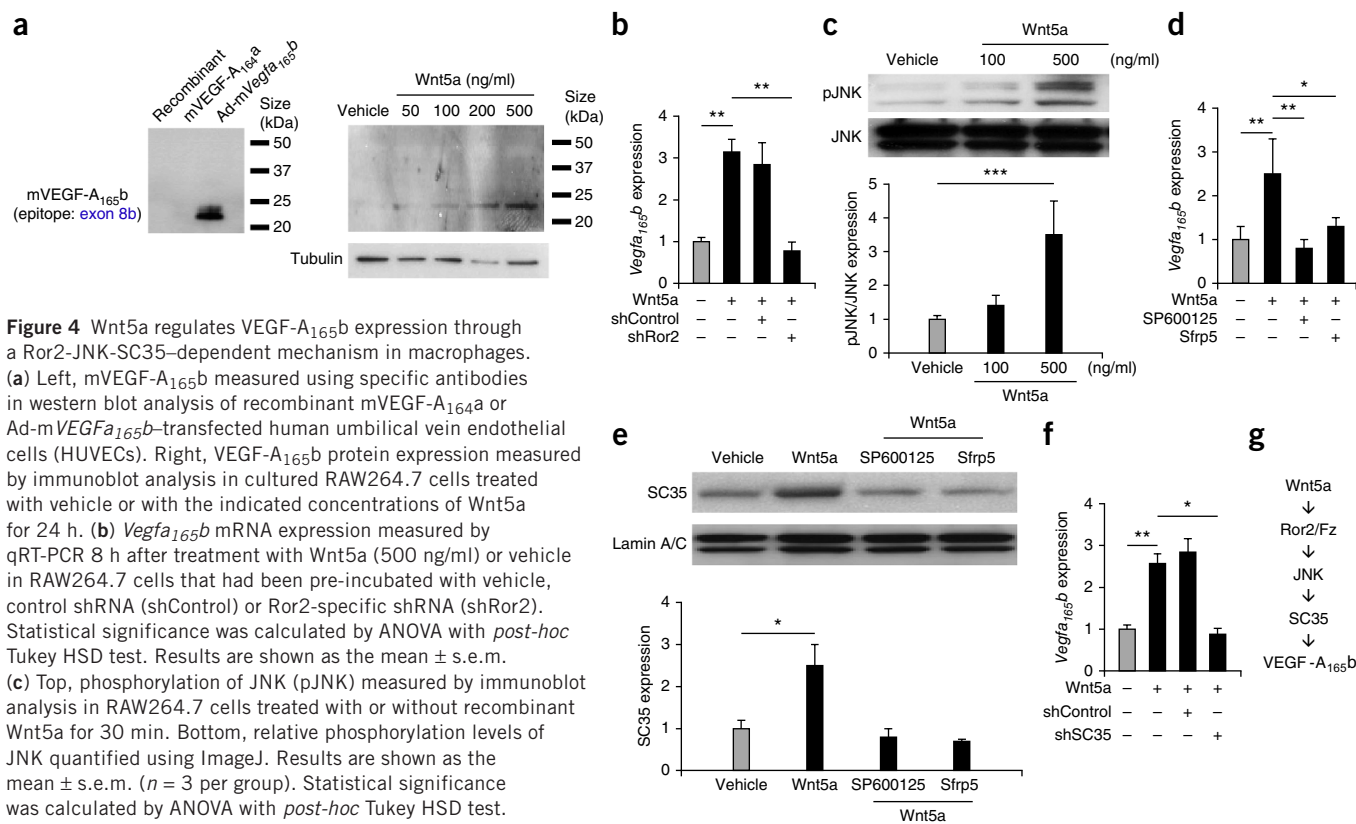
Figure 4 Wnt5a regulates VEGF-A$_{165}$b expression through a Ror2-JNK-SC35–dependent mechanism in macrophages. (**a**) Left, mVEGF-A$_{165}$b measured using specific antibodies in western blot analysis of recombinant mVEGF-A$_{164}$a or Ad-m$Vegfa_{165}$b–transfected human umbilical vein endothelial cells (HUVECs). Right, VEGF-A$_{165}$b protein expression measured by immunoblot analysis in cultured RAW264.7 cells treated with vehicle or with the indicated concentrations of Wnt5a for 24 h. (**b**) $Vegfa_{165}$b mRNA expression measured by qRT-PCR 8 h after treatment with Wnt5a (500 ng/ml) or vehicle in RAW264.7 cells that had been pre-incubated with vehicle, control shRNA (shControl) or Ror2-specific shRNA (shRor2). Statistical significance was calculated by ANOVA with *post-hoc* Tukey HSD test. Results are shown as the mean ± s.e.m. (**c**) Top, phosphorylation of JNK (pJNK) measured by immunoblot analysis in RAW264.7 cells treated with or without recombinant Wnt5a for 30 min. Bottom, relative phosphorylation levels of JNK quantified using ImageJ. Results are shown as the mean ± s.e.m. (*n* = 3 per group). Statistical significance was calculated by ANOVA with *post-hoc* Tukey HSD test. (**d**) $Vegfa_{165}$b mRNA expression measured by qRT-PCR in RAW264.7 cells treated with or without Wnt5a, or with either SP600125 (10 μM) or recombinant Sfrp5 (1 μg/ml) added 10 min before the addition of recombinant Wnt5a for 8 h. Results are shown as the mean ± s.e.m. (*n* = 3 per group). Statistical significance was calculated by ANOVA with *post-hoc* Tukey HSD test. (**e**) Top, SC35 protein expression measured by immunoblot analysis in the presence or absence of recombinant Wnt5a in RAW264.7 cells. The effects of the JNK inhibitor SP600125 (10 μM) or Sfrp5 (1 μg/ml) added 10 min before Wnt5a-induced SC35 expression were evaluated at 1 h. Bottom, relative levels of SC35 quantified using ImageJ. Protein levels were normalized using lamin A/C as the loading control. Results are shown as the mean ± s.e.m. (*n* = 3 per group). Statistical significance was calculated by ANOVA with *post-hoc* Tukey HSD test. (**f**) $Vegfa_{165}$b mRNA expression measured by qRT-PCR in RAW264.7 cells treated with shControl or shSC35 for 8 h and then treated with or without recombinant Wnt5a for 8 h. Statistical significance was calculated by ANOVA with *post-hoc* Tukey HSD test. Results are shown as the mean ± s.e.m. (**g**) Schematic of the proposed mechanism involving Wnt5a-induced VEGF-A$_{165}$b expression through ROR2/FZ, JNK and SC35. *$P < 0.05$, **$P < 0.01$, ***$P < 0.001$.

expression, both in the ischemic tissue and in the serum, an increase in the levels of mVEGF-A$_{165}$b but no increase in the levels of mVEGF-A$_{164}$a (**Supplementary Fig. 14g,h**). Assessment of isoform-specific qPCR of transcripts in the ischemic and non-ischemic gastrocnemius muscle revealed a modest upregulation of the exon 8a–containing m$Vegfa_{164}$a isoform in WT mice after surgery. However, the exon 8b–containing m$Vegfa_{165}$b isoform was selectively upregulated in the ischemic muscle of Sfrp5 KO mice (**Supplementary Fig. 14i**). To assess the functional importance of mVEGF-A$_{165}$b upregulation, we administered the VEGF-A$_{165}$b–neutralizing antibody or control IgG to Sfrp5 KO mice before hind limb surgery. Ischemic limbs of Sfrp5 KO mice receiving the neutralizing antibody had increased reperfusion, as determined by LDBF (**Supplementary Fig. 14j**) and an increase in capillary density in the gastrocnemius muscle of the ischemic limb relative to the contralateral control limb; in contrast, Sfrp5 KO mice treated with IgG showed no increase in capillary density (**Supplementary Fig. 14j**). Collectively, these data indicate that the antiangiogenic mVEGF-A$_{165}$b splice variant is upregulated in response to ischemia in both Sfrp5 KO and LysM-Wnt5a^{GOF} mice and that this upregulation contributes to an impaired angiogenic response.

PAD is strongly associated with diabetes mellitus[26], and studies in experimental models have shown that metabolic dysfunction

leads to a reduction in the angiogenic response to tissue ischemia[27]. Because perturbations in the Sfrp5-Wnt5a regulatory system contribute to systemic metabolic dysfunction under conditions of obesity[25], we evaluated the regulation and function of the antiangiogenic mVEGF-A$_{165}$b isoform in models of diet-induced obesity and leptin deficiency. Consistent with observations in adipose tissue[25], Wnt5a protein and mRNA expression were elevated in the ischemic muscle of mice fed a high fat and high sucrose (HF/HS) diet or ob/ob mice relative to mice fed a standard chow diet or C57BL/6J mice, respectively (**Fig. 3a,b** and **Supplementary Fig. 15a,b**). The increase in Wnt5a expression in muscle tissue under conditions of metabolic dysfunction was associated with an increase in the infiltration of Wnt5a and Mac2 double-positive macrophages (**Fig. 3c** and **Supplementary Fig. 15c**). Western blot analysis of gastrocnemius muscle from these experimental groups of mice revealed upregulation of VEGF-A expression in both the HF/HS-fed and ob/ob mice using a pan–VEGF-A antibody that does not discriminate between the isoforms (**Fig. 3d** and **Supplementary Fig. 15d**). Isoform-specific antibodies revealed modest upregulation of the mVEGF-A$_{164}$a isoform in ischemic limbs of metabolically normal mice; in contrast, the HF/HS-fed and ob/ob mice displayed marked elevations in the levels of the antiangiogenic mVEGF-A$_{165}$b isoform (**Fig. 3d** and **Supplementary Fig. 15d**). Using antibodies specific for the unique

VEGF-Ax extension peptide or the exon 8b–encoded hexapeptide, we detected exon 8b–containing but no Ax extension peptide–containing material in ob/ob mice (**Supplementary Fig. 15e**) or HF/HS-fed mice (data not shown) under the conditions of our assays. Corroborating the findings with the isoform-specific antibodies, isoform-specific qPCR of *Vegfa* cDNA isolated from gastrocnemius muscle revealed that metabolic dysfunction led to reduced expression of the proangiogenic *Vegfa* isoform and increased expression of the antiangiogenic exon 8b–containing isoform (**Fig. 3e** and **Supplementary Fig. 15f**). HF/HS-fed and ob/ob mice both displayed impaired revascularization as assessed by LDBF imaging and capillary and arteriole density analyses (**Fig. 3f** and **Supplementary Figs. 15g** and **16**). To assess the functional importance of mVEGF-A_{165}b under these conditions of metabolic dysfunction, we treated both ob/ob and HF/HS-fed C57BL/6 mice with VEGF-A_{165}b–neutralizing antibody or IgG control and subjected them to hind limb ischemic surgery. Whereas the neutralizing antibody had no effect on the angiogenic response in metabolically normal mice, antibody treatment of both the ob/ob and HF/HS-fed mice led to significant improvements in ischemic limb revascularization (**Fig. 3f** and **Supplementary Figs. 15g** and **16**).

To examine how VEGF-A_{165}b expression is regulated at a mechanistic level, we treated cultured RAW264.7 cells, a mouse macrophage line, with recombinant Wnt5a. Wnt5a stimulation led to a dose-dependent increase in VEGF-A_{165}b levels (**Fig. 4a**), as well as upregulation of the *Vegfa$_{165}$b* splice variant at the mRNA level (**Fig. 4b**). Consistent with previous work showing that Wnt5a signals in a noncanonical manner[28], knockdown of Ror2, a Frizzled co-receptor protein, abolished Wnt5a-mediated *Vegfa$_{165}$b* induction (**Fig. 4b**). Also consistent with a noncanonical signaling mechanism, Wnt5a treatment led to the activation of JNK (**Fig. 4c**), and pretreatment with the JNK inhibitor SP600125 abolished Wnt5a-mediated *Vegfa$_{165}$b* expression (**Fig. 4d**). Similarly, treatment with recombinant Sfrp5 protein blocked VEGF-A_{165}b expression under these conditions (**Fig. 4d**). Further investigation revealed that Wnt5a upregulated the expression of SC35, a pre-mRNA splicing factor implicated in the alternative processing of *Vegfa* at exon 8 (ref. 29), in a JNK- and Sfrp5-dependent manner (**Fig. 4e**). Knockdown of SC35 blocked Wnt5a-mediated induction of *Vegfa$_{165}$b* (**Fig. 4f**). Collectively, these data indicate that Wnt5a promotes the processing of *Vegfa* to yield the exon 8b–containing isoform, at least in part, through an Ror2-JNK-SC35–dependent mechanism (**Fig. 4g**).

Here we show that the antiangiogenic splice variant of VEGF-A is expressed in clinical and experimental settings that are associated with impaired vascularization. It has been noted previously, and confirmed here, that total VEGF-A levels are paradoxically elevated in patients with PAD[2,9]. Using isoform-specific antibodies, we provide evidence that circulating VEGF-A in patients with PAD is comprised predominantly of the variant VEGF-A_{165}b isoform. In mouse experimental models, we established the presence of mVEGF-A_{165}b and demonstrated upregulation of its expression under conditions of systemic metabolic dysfunction. In contrast, we did not detect the VEGF-Ax isoform under these conditions. Although VEGF-Ax was present in human serum, we did not observe its upregulation in a small cohort of patients with PAD. However, VEGF-Ax levels should be further evaluated using a larger number of patients, as well as different metabolic phenotypes. We also demonstrated that the VEGF-A_{165}b isoform impairs revascularization in an experimental model of PAD. Conversely, acute immunological neutralization of mVEGF-A_{165}b promotes revascularization of ischemic tissue under conditions in which the process of regenerative angiogenesis is impaired. These findings support the concept that VEGF-A_{165}b may serve as a new pharmacological target to treat limb ischemia in patients with PAD and that its neutralization may augment the activities of proangiogenic growth factors.

Metabolic diseases, including diabetes and obesity, contribute to ischemic cardiovascular disease, but the molecular mechanisms underlying this pathological connection remain incompletely defined. Obesity-linked changes in the expression of adipose tissue–derived Sfrp5 can lead to overactivation of noncanonical Wnt5a signaling in macrophages that, in turn, promotes inflammation and systemic metabolic dysfunction, but the link between this signaling and vascular disease had not previously been identified[25]. We now show that Sfrp5 deficiency impairs the hind limb revascularization response to ischemia. This impairment is associated with greater infiltration of activated, Wnt5a-positive macrophages in the ischemic tissue. Myeloid-specific Wnt5a overexpression parallels Sfrp5 deficiency, with exaggerated macrophage infiltration and blunted revascularization in ischemic limbs. In both models, we demonstrated upregulation of the mVEGF-A_{165}b isoform in ischemic tissue and showed that immunological neutralization of this inhibitory VEGF-A isoform promotes the angiogenic response to ischemia. These data indicate that Wnt5a, and its upstream effector Sfrp5, mediate the effects of metabolic dysfunction on regenerative angiogenesis by controlling macrophage expression of VEGF-A_{165}b. Taken together, our findings identify the Sfrp5–Wnt5a–VEGF-A_{165}b axis as a regulator of the vascular response to ischemia in the setting of metabolic disease and provide a new potential mechanism for the link between obesity and cardiovascular disease.

METHODS

Methods and any associated references are available in the online version of the paper.

Note: Any Supplementary Information and Source Data files are available in the online version of the paper.

AUTHOR CONTRIBUTIONS
All authors participated in the analysis and interpretation of data. R.K. and N.M.H. performed the statistical analyses of the human and mouse data. R.K. and K.W. conceived the project and designed the experiments. K.N., S.M., D.T.-M.N., I.S., J.J.F., Y.K., S.Y., Y.Q., T. Matsushita, T. Murohara, N.G., D.O.B. and R.K. conducted experiments. R.K., T.P.Y., Y.Q. and D.O.B. developed experimental tools or mouse models. R.K., N.M.H. and K.W. wrote and edited the manuscript.

1. Blann, A.D. *et al.* Vascular endothelial growth factor and its receptor, Flt-1, in the plasma of patients with coronary or peripheral atherosclerosis, or type II diabetes. *Clin. Sci. (Lond.)* **102**, 187–194 (2002).

2. Findley, C.M., Mitchell, R.G., Duscha, B.D., Annex, B.H. & Kontos, C.D. Plasma levels of soluble Tie2 and vascular endothelial growth factor distinguish critical limb ischemia from intermittent claudication in patients with peripheral arterial disease. *J. Am. Coll. Cardiol.* **52**, 387–393 (2008).

3. Murray, C.J. *et al.* Disability-adjusted life years (DALYs) for 291 diseases and injuries in 21 regions, 1990–2010: a systematic analysis for the Global Burden of Disease Study 2010. *Lancet* **380**, 2197–2223 (2012).

4. Hamburg, N.M. & Balady, G.J. Exercise rehabilitation in peripheral artery disease: functional impact and mechanisms of benefits. *Circulation* **123**, 87–97 (2011).

5. Anderson, P.L. *et al.* Understanding trends in inpatient surgical volume: vascular interventions, 1980–2000. *J. Vasc. Surg.* **39**, 1200–1208 (2004).

6. Go, A.S. *et al.* Heart disease and stroke statistics—2013 update: a report from the American Heart Association. *Circulation* **127**, e6–e245 (2013).

7. Duscha, B.D. *et al.* Angiogenesis in skeletal muscle precede improvements in peak oxygen uptake in peripheral artery disease patients. *Arterioscler. Thromb. Vasc. Biol.* **31**, 2742–2748 (2011).

8. Carmeliet, P. & Jain, R.K. Molecular mechanisms and clinical applications of angiogenesis. *Nature* **473**, 298–307 (2011).

9. Makin, A.J., Chung, N.A., Silverman, S.H. & Lip, G.Y. Vascular endothelial growth factor and tissue factor in patients with established peripheral artery disease: a link between angiogenesis and thrombogenesis? *Clin. Sci. (Lond.)* **104**, 397–404 (2003).

10. Mäkinen, K. *et al.* Increased vascularity detected by digital subtraction angiography after VEGF gene transfer to human lower limb artery: a randomized, placebo-controlled, double-blinded phase II study. *Mol. Ther.* **6**, 127–133 (2002).

11. Rajagopalan, S. *et al.* Regional angiogenesis with vascular endothelial growth factor in peripheral arterial disease: a phase II randomized, double-blind, controlled study of adenoviral delivery of vascular endothelial growth factor 121 in patients with disabling intermittent claudication. *Circulation* **108**, 1933–1938 (2003).

12. Bates, D.O. *et al.* Association between VEGF splice isoforms and progression-free survival in metastatic colorectal cancer patients treated with bevacizumab. *Clin. Cancer Res.* **18**, 6384–6391 (2012).

13. Kawamura, H., Li, X., Harper, S.J., Bates, D.O. & Claesson-Welsh, L. Vascular endothelial growth factor (VEGF)-A165b is a weak *in vitro* agonist for VEGF receptor-2 due to lack of coreceptor binding and deficient regulation of kinase activity. *Cancer Res.* **68**, 4683–4692 (2008).

14. Bates, D.O. *et al.* VEGF165b, an inhibitory splice variant of vascular endothelial growth factor, is down-regulated in renal cell carcinoma. *Cancer Res.* **62**, 4123–4131 (2002).

15. Harper, S.J. & Bates, D.O. VEGF-A splicing: the key to anti-angiogenic therapeutics? *Nat. Rev. Cancer* **8**, 880–887 (2008).

16. Cébe Suarez, S. *et al.* A VEGF-A splice variant defective for heparan sulfate and neuropilin-1 binding shows attenuated signaling through VEGFR-2. *Cell. Mol. Life Sci.* **63**, 2067–2077 (2006).

17. Jones, W.S. *et al.* Alteration in angiogenic and anti-angiogenic forms of vascular endothelial growth factor-A in skeletal muscle of patients with intermittent claudication following exercise training. *Vasc. Med.* **17**, 94–100 (2012).

18. Dokun, A.O. & Annex, B.H. The VEGF165b "ICE-o-form" puts a chill on the VEGF story. *Circ. Res.* **109**, 246–247 (2011).

19. Eswarappa, S.M. *et al.* Programmed translational readthrough generates antiangiogenic VEGF-Ax. *Cell* **157**, 1605–1618 (2014).

20. McDermott, M.M. *et al.* Elevated levels of inflammation, d-dimer, and homocysteine are associated with adverse calf muscle characteristics and reduced calf strength in peripheral arterial disease. *J. Am. Coll. Cardiol.* **50**, 897–905 (2007).

21. Vidula, H. *et al.* Biomarkers of inflammation and thrombosis as predictors of near-term mortality in patients with peripheral arterial disease: a cohort study. *Ann. Intern. Med.* **148**, 85–93 (2008).

22. Stefater, J.A. III *et al.* Regulation of angiogenesis by a non-canonical Wnt-Flt1 pathway in myeloid cells. *Nature* **474**, 511–515 (2011).

23. Kendall, R.L. & Thomas, K.A. Inhibition of vascular endothelial cell growth factor activity by an endogenously encoded soluble receptor. *Proc. Natl. Acad. Sci. USA* **90**, 10705–10709 (1993).

24. Tischer, E. *et al.* The human gene for vascular endothelial growth factor. Multiple protein forms are encoded through alternative exon splicing. *J. Biol. Chem.* **266**, 11947–11954 (1991).

25. Ouchi, N. *et al.* Sfrp5 is an anti-inflammatory adipokine that modulates metabolic dysfunction in obesity. *Science* **329**, 454–457 (2010).

26. Marso, S.P. & Hiatt, W.R. Peripheral arterial disease in patients with diabetes. *J. Am. Coll. Cardiol.* **47**, 921–929 (2006).

27. Schiekofer, S., Galasso, G., Sato, K., Kraus, B.J. & Walsh, K. Impaired revascularization in a mouse model of type 2 diabetes is associated with dysregulation of a complex angiogenic-regulatory network. *Arterioscler. Thromb. Vasc. Biol.* **25**, 1603–1609 (2005).

28. Ho, H.Y. *et al.* Wnt5a-Ror-Dishevelled signaling constitutes a core developmental pathway that controls tissue morphogenesis. *Proc. Natl. Acad. Sci. USA* **109**, 4044–4051 (2012).

29. Merdzhanova, G. *et al.* The transcription factor E2F1 and the SR protein SC35 control the ratio of pro-angiogenic versus antiangiogenic isoforms of vascular endothelial growth factor-A to inhibit neovascularization *in vivo*. *Oncogene* **29**, 5392–5403 (2010).

ONLINE METHODS

Clinical samples. Patients with PAD (defined as ankle-brachial index <0.9 or prior revascularization) and control individuals without PAD (ankle-brachial index >1.0 and <1.4) were enrolled from outpatient clinics at Boston Medical Center. The Boston Medical Center Institutional Review Board approved the study, and all participants provided written informed consent. Ankle-brachial index was measured using a Doppler probe to record systolic pressure in the brachial, posterior tibial and dorsalis pedis arteries and by obtaining the ratio of ankle to arm pressure. The lowest leg ankle-brachial index is reported[30]. On the day of the visit, fasting blood samples were obtained to measure lipids and glucose. PBMCs were isolated by density gradient centrifugation in Vacutainer cell preparation tubes (CPT tubes with sodium citrate, Becton-Dickinson), treated with an RNA stabilizer (RNAlater, Qiagen) and stored at −80 °C before RNA isolation.

ELISA. Total circulating levels of VEGF-A from patients with PAD and healthy subjects and in mouse serum after hind limb ischemia were measured with quantitative colorimetric sandwich ELISAs (R&D Systems, human: DVE00, mouse: MMV00). Circulating levels of mouse sFlt-1 in WT, LysM-Wnt5a^{GOF} and Sfrp5 KO mice were measured with a quantitative colorimetric sandwich ELISA (R&D Systems, MVR100). For all ELISAs, protein concentrations were calculated using a standard curve generated with recombinant standards provided by the manufacturer. Optical density was measured using a microtiter plate reader at 450 nm. Each sample was measured in duplicate and averaged.

Human monocyte isolation. The Human Monocyte Isolation Kit II (Miltenyi Biotech) was used to magnetically separate monocytes from non-monocytes following the manufacturer's recommendations. Non-monocyte cells in PBMC samples were magnetically labeled using a cocktail of antibodies against the non-monocyte antigens CD3, CD7, CD16, CD19, CD56, CD123 and glycophorin A. Monocyte (unlabeled) and non-monocyte (labeled) fractions were then separated with Miltenyi MS columns and a MiniMacs separator.

Mice. Mice with myeloid-restricted Wnt5a overexpression were generated by crossing lysozyme M–Cre (LysM-Cre) mice (Jackson Laboratories, stock number 004781) with knock-in mice carrying a Cre-inducible Wnt5a transgene (**Supplementary Fig. 5a**). Mice (C57BL/6, Charles River Laboratory) were fed either a standard chow diet (Harlan Teklad global 18% protein rodent diet, #2018) or a HF/HS diet (Bio-Serv, #F1850)[25], as indicated. The composition of the HF/HS diet was 35.8% fat (primarily lard), 36.8% carbohydrate (primarily sucrose) and 20.3% protein. For the feeding of the high-caloric diet, 4-week-old mice were maintained on a HF/HS diet for 8 weeks. Mice lacking Sfrp5 were described previously[25]. Sfrp5 KO mice and C57BL/6J WT mice were used in this study. ob/ob (stock number 000632), 8-week-old male mice were purchased from Jackson Laboratory. Study protocols were approved by the Boston University Institutional Animal Care and Use Committee.

Reagents. Recombinant human VEGF-A$_{165}$ (293-VE-010), human VEGF-A$_{165}$b (3045-VE-025), mouse VEGF-A$_{164}$ (493-MV-025), human (6266-SF-050) and mouse Sfrp5 (7195-SF-050) and human/mouse Wnt5a (645-WN-010) were purchased from R&D systems. Polyhistidine-tagged VEGF-Ax$_{Ala}$ was prepared from HEK292-6E cells as described previously[19]. α-tubulin antibody (11H10, 1:1,000) was purchased from Cell Signaling Technology. Wnt5a antibody (MAB645, 1:250) was purchased from R&D Systems. Lamin A/C (#2032, 1:1,000), JNK (#9252, 1:500), pJNK (Thr183/Tyr185, #9912, 1:500), VEGFR2 and pVEGFR2 (Tyr951, 1:500) antibodies were purchased from Cell Signaling Technology. SC35 antibody (#556363, 1:500) was purchased from BD Pharmingen. VEGF-A (A-20, sc-152, 1:1,000), phosphotyrosine (PY99, 1:200), Flk-1 (VEGFR2; A-3, 1:1,000) and galectin-3 (H-160, 1:1,000) antibodies were purchased from Santa Cruz Biotechnology. The immunogen for the VEGF-A antibody, sc-152, maps within amino acids 1–50 at the N terminus of human VEGF-A (protein accession P15692). The A-20 antibody cross reacts with all human and mouse VEGF-A isoforms. A neutralizing monoclonal antibody against human VEGF-A$_{165}$b was generated by immunizing 6- to 8-week-old female BALB/c mice with a synthetic peptide fragment corresponding to the nine-amino-acid C-terminal sequence of VEGF-A$_{165}$b (TCRSLTRKD) coupled to keyhole limpet hemocyanin (KLH). Specificity was determined by immunoblot analysis using recombinant VEGF-A$_{165}$b and VEGF-A$_{165}$a (data not shown). A C-terminal (exon 8b)-specific antibody was purchased from Abcam. A polyclonal antibody specific to the C terminus (exon 8a) of human VEGF-A$_{165}$a was generated by immunization of a rabbit with a KLH-conjugated peptide, TCRCDKPRR, corresponding to the last nine amino acids of VEGF-A$_{165}$a, using standard immunization techniques. IgG was affinity purified from plasma and its selectivity determined by immunoblotting (data not shown). A polyclonal antibody specific to the C terminus (exon 8b) of mouse VEGF-A$_{165}$b was generated by immunizing rabbits with a combination of two synthetic peptides (CRPLTGKTD-OH conjugated to KLH and unconjugated acetyl-QSKNILMQYIKANSFIGITELCRPLTGKTD-OH) (21st Century Biochemicals). A polyclonal antibody against VEGF-Ax was generated by immunizing a rabbit with the synthetic KLH-conjugated peptide, AGLEEGASLRVSGTR, that is not present in the VEGF-A$_{165}$b isoform[19].

Conventional PCR and qRT-PCR. mRNA was extracted from human mononuclear cells and gastrocnemius muscle tissue of mice using an RNeasy Mini Kit (Qiagen) according to the manufacturer's protocol. cDNA was produced using 1 μg of starting mRNA and the QuantiTect Reverse Transcription Kit (Qiagen) as directed by the manufacturer. Conventional PCR was performed to differentiate between exon 8a– and 8b–containing isoforms. Taking advantage of the fact that the exon 8b–containing isoform is 66-bp shorter than the exon 8a–containing isoform, human and mouse primers were designed to amplify the region spanning the proximal and distal splice sites in human *VEGFA$_{165}$a* and *VEGFA$_{165}$b* and in mouse *Vegfa$_{164}$a* and *Vegfa$_{165}$b* (**Supplementary Fig. 7**). Conventional PCR analysis was performed using the following conditions: 96 °C for 2 min followed by 45 cycles at 96 °C for 30 s, 60 °C for 30 s and 72 °C for 30 s. The primers used were 5′-AAGGCGAGGCAGCTTGAGTTA-3′ and 5′-TCAGTCTTTCCTGGTGAGAG-3′ for human *VEGFA$_{165}$a* and *VEGFA$_{165}$b* and 5′-CAGAAAATCACTGTGAGCCTTGTT-3′ and 5′-ATT AAGGACTGTTCTGTCAA-3′ for mouse *Vegfa$_{164}$a* and *Vegfa$_{165}$b*. Exon-specific qRT-PCR was performed with the Applied Biosystems VIIA7 real-time PCR detection system using SYBR Green I as a double-strand DNA–specific dye according to the manufacturer's instructions (Applied Biosystems). Primers were designed to recognize the exon 5/7 junction and the 7/8a or 7/8b junction. mRNA levels were expressed relative to the levels of *GAPDH*. Real-time RT-PCR analysis was performed using the following conditions: 95 °C for 10 min followed by 45 cycles at 95 °C for 15 s, 64 °C for 30 s and 72 °C for 30 s. Other primer sequences used are described in **Supplementary Table 2**.

Immunoblot analysis. Clinical serum samples were resolved by SDS-PAGE. Mouse gastrocnemius muscle tissue samples obtained on day 3 or 7 after surgery were homogenized in lysis buffer containing 20 mM Tris-HCl (pH 8.0), 1% Nonidet P-40, 150 mM NaCl, 0.5% deoxycholic acid, 1 mM sodium orthovanadate and a protease and phosphatase inhibitor cocktail (Thermo Scientific). Protein content was determined by the Bradford method. Equal amounts of protein lysates were resolved by SDS-PAGE. The membranes were immunoblotted with the indicated antibodies at a 1:1,000 dilution followed by the secondary antibody conjugated to horseradish peroxidase at a 1:1,000–5,000 dilution. An ECL western blotting detection kit (Thermo Scientific) was used for detection. Protein levels quantitated from immunoblots were normalized using loading controls.

Immunoprecipitation. Immunoprecipitation was performed using magnetic beads coated with sheep anti-rabbit IgGs (Dynabeads M-280, Dynal) or protein G from the Dynabeads immunoprecipitation kit (10007D, Life Technologies). Beads were incubated overnight at 4 °C with rabbit anti-mouse VEGF-A$_{165}$b antibody (1 μg antibody for 4×10^7 beads) in PBS and 1% skim milk, followed by overnight incubation at 4 °C with 100 μg protein in the presence of a protease and phosphatase inhibitor cocktail (Thermo Scientific). Bound proteins were eluted from the beads by boiling in 25 μl of SDS-PAGE sample buffer.

PAD model of revascularization. WT, LysM-Wnt5a^{GOF} and Sfrp5 KO mice (both in a C57BL/6J background), HF/HS-fed (C57BL/6 background) and

ob/ob (C57BL/6J background) mice were used for this study. Male mice between 10 and 12 weeks of age were subjected to unilateral hind limb surgery under anesthesia with sodium pentobarbital (50 mg/kg body weight intraperitoneally). The left femoral artery and vein were excised gently from the proximal portion of the femoral artery to the distal portion of the saphenous artery. The remaining arterial branches, including the perforator arteries, were also excised. After excision of the femoral artery as previously described[31], hind limb blood flow recovery was monitored in real time by laser Doppler imaging (LDI) (Moor LDI, Moor Instruments)[32] before surgery and on days 0, 3, 7, 14, 21 and 28 after surgery by an investigator blinded to the experimental group. To avoid data variability due to ambient light and temperature, hind limb blood flow is expressed as the ratio of left (ischemic) to right (non-ischemic) LDBF.

Immunohistochemistry. Muscle samples were imbedded in Tissue Tek optimal cutting temperature (OCT) compound (VWR) and snap frozen in liquid nitrogen. Tissue slices (5 µm in thickness) were prepared. Gastrocnemius muscles were processed for immunohistochemistry of CD31, Wnt5a and Mac2. The primary antibodies for CD31 (1:50, Becton Dickinson), Wnt5a (1:200, R&D Systems) and Mac2 (1:500, Santa Cruz Biotechnology) were applied to the sections overnight at 4 °C. After washing, the sections were sequentially incubated with appropriate FITC- or PE-conjugated secondary antibodies (Invitrogen) for 1 h. Digital images of five microscopic fields from four different sections from each animal were scored.

Anatomical analyses. Capillary density within the thigh gastrocnemius muscle was quantified by histological analysis as described previously[31]. Capillary density is expressed as the number of CD31-positive cells per high-power field. Arteriole density analysis was quantified in fresh-frozen sections of hind limb gastrocnemius muscle at day 28 after ischemic surgery. Arteriole density is expressed as the number of α-smooth muscle actin (aSMA)-positive cells per high-power field. Immunostains were visualized using 3,3′-diaminobenzidine (DAB).

Adenoviral vectors. Full-length mouse $Vegfa_{164}a$ and $Vegfa_{165}b$ cDNAs were each subcloned into an adenoviral shuttle CMV vector (AdEasy system, Agilent Technologies). Adenoviral vectors expressing mouse VEGF-A$_{164}$a and VEGF-A$_{165}$b (Ad-$Vegfa_{164}a$ and Ad-$Vegfa_{165}b$) were constructed under the control of the CMV promoter (**Supplementary Fig. 11a**)[31]. Ad-m$Vegfa_{165}b$ or Ad–$β$-gal (control) was injected into the jugular vein of WT mice ($2 × 10^9$ PFU in each group) 3 d before ischemic surgery (**Fig. 2h**).

VEGF-A$_{165}$b–neutralizing antibody. Anti-human VEGF-A$_{165}$b–neutralizing monoclonal antibody (100 µg) was injected intraperitoneally into mice on days 0, 3 and 7 after surgery. As a control, nonspecific mouse IgG (sc-2027, Santa Cruz Biotechnology) was administered in a similar manner.

Cell culture. HEK293A cells (ATCC) were grown in DMEM (10% FBS). HEK293A cells were trypsinized and counted, and virus (Ad-m$Vegfa_{164}a$ and Ad-$mVegfa_{165}b$) was added at the indicated multiplicity of infection. RNA was isolated from infected cells after 48 h of infection (**Supplementary Fig. 9**). RAW264.7 cells (TIB-71, American Type Culture Collection) were grown in DMEM supplemented with 10% FBS and antibiotics. RAW264.7 cells were treated with recombinant Wnt5a (500 ng/ml) for the indicated lengths of time. HUVECs (American Type Culture Collection) of passages 3–5 were cultured in endothelial growth medium 2 (EGM-2; Lonza). HUVECs were trypsinized and counted, and virus (Ad-m$Vegfa_{164}a$ and Ad-m$Vegfa_{165}b$) was added at a multiplicity of infection of 100. Protein was isolated from the transfected cells after 72 h of infection. For some experiments, HUVECs were infected with Ad-m$Vegfa_{165}b$ at a multiplicity of infection of 100 for 24 h, followed by a medium change and collection of the conditioned medium. The conditioned medium was concentrated by Centrifugal Filter Units (Amicon Ultra-15 Centrifugal Filter Devices, Millipore) (**Supplementary Fig. 13**). Lentiviral plasmids expressing a ROR2-specific shRNA (5′-CCGGCGTGGTGCTTTA CGCAGAATACTCGAGTATTCTGCGTAAAGCACCACGTTTTT-3′) or a SC35-specific shRNA (5′-CCGGAGTCCAGATCTGCCCGAAGATCTCGA GATCTTCGGGCAGATCTGGACTTTTTTG-3′) in the pLKO.1-puro vector were purchased from Sigma-Aldrich. Lentivirus expressing scrambled shRNA was used as a negative control. Recombinant lentiviruses were produced by co-transfecting the pLKO.1-scramble, pLKO.1–mouse ROR2 or pLKO.1–mouse SC35 shRNA plasmids with the MISSION Lentiviral Packaging Mix (SHP001, Sigma-Aldrich) into HEK293T cells (American Type Culture Collection) using Lipofectamine 2000 (Invitrogen). The medium was replaced after 24 h, and viral supernatants were harvested 2 d after transfection and stored at −80 °C. For infection, RAW264.7 cells were seeded at a density of $2.5 × 10^5$ cells per well of a six-well plate coated with poly-L-lysine and infected with viral supernatant at a 100–200 multiplicity of infection containing 5 µg/ml Polybrene. The medium was replaced the next day. Cells were cultured for an additional 72 h and used for experiments.

Statistical analyses. Statistical analyses were completed with SPSS 20.0. VEGF-A isoform levels and clinical characteristics were evaluated for normality by examining histograms and quantile-quantile plots by performing Shapiro-Wilk tests. Clinical characteristics were compared between patients with PAD and controls using independent sample t tests or $χ^2$ tests as appropriate. Circulating VEGF-A$_{165}$b expression was compared with PBMC expression and ankle-brachial index using Spearman correlations. Additional analytic methods are included in the figure legends. Data are presented as the mean ± s.e.m., as indicated in the figure legends. Two-sided P values of <0.05 were considered statistically significant. No statistical method was used to predetermine sample size. No randomization was used in the animal experiments.

30. Aboyans, V. *et al.* Measurement and interpretation of the ankle-brachial index: a scientific statement from the American Heart Association. *Circulation* **126**, 2890–2909 (2012).
31. Ouchi, N. *et al.* Follistatin-like 1, a secreted muscle protein, promotes endothelial cell function and revascularization in ischemic tissue through a nitric-oxide synthase–dependent mechanism. *J. Biol. Chem.* **283**, 32802–32811 (2008).
32. Kikuchi, R. *et al.* Pitavastatin-induced angiogenesis and arteriogenesis is mediated by Notch1 in a murine hind limb ischemia model without induction of VEGF. *Lab. Invest.* **91**, 691–703 (2011).